Journal of Computational Neuroscience 9, 49–65, 2000

Synchronous Clusters in a Noisy Inhibitory Neural Network

P.H.E. TIESINGA
Sloan Center for Theoretical Neurobiology, Salk Institute, 10010 North Torrey Pines Road, La Jolla, CA 92037; Center for Interdisciplinary Research on Complex Systems, and Department of Physics, Northeastern University, Boston MA 02115
tiesinga@salk.edu

JORGE V. JOSÉ
Center for Interdisciplinary Research on Complex Systems, and Department of Physics, Northeastern University, Boston MA 02115
jjv@neu.edu

Received December 29, 1998; Revised July 12, 1999; Accepted August 5, 1999

Action Editor: G. Bard Ermentrout

Abstract. We study the stability and information encoding capacity of synchronized states in a neuronal network model that represents part of thalamic circuitry. Our model neurons have a Hodgkin-Huxley-type low-threshold calcium channel, display postinhibitory rebound, and are connected via GABAergic inhibitory synapses.

We find that there is a threshold in synaptic strength, τ_c, below which there are no stable spiking network states. Above threshold the stable spiking state is a cluster state, where different groups of neurons fire consecutively, and each neuron fires with the same cluster each time. Weak noise destabilizes this state, but stronger noise drives the system into a different, self-organized, stochastically synchronized state. Neuronal firing is still organized in clusters, but individual neurons can hop from cluster to cluster. Noise can actually induce and sustain such a state below the threshold of synaptic strength. We do find a qualitative difference in the firing patterns between small ($\sim$10 neurons) and large ($\sim$1000 neurons) networks.

We determine the information content of the spike trains in terms of two separate contributions: the spike-time jitter around cluster firing times, and the hopping from cluster to cluster. We quantify the information loss due to temporally correlated interspike intervals. Recent experiments on the locust olfactory system and striatal neurons suggest that the nervous system may actually use these two channels to encode separate and unique information.

Keywords: inhibition, neural network, synchronization, noise, information

1. Introduction

The brain receives an enormous amount of information transduced by peripheral sense organs. This massive information influx is coded and decoded in ways that are not yet fully understood in cognitive neuroscience. Recent studies have focused on specific neural substrates for binding mechanisms. Binding is the process by which the brain combines different aspects of sensory modalities of one object into one unified percept. The neural mechanisms that underlie synchronization in different parts of the brain are only partly understood. There is the suggestion that synchronization may be relevant to binding (Singer and Gray, 1995). Recent experiments have shown that inhibitory interneurons in the hippocampus (Whittington et al., 1995), the thalamic reticular nucleus (Steriade et al., 1993), and the locust olfactory system (MacLeod and Laurent, 1996)

can indeed synchronize neuronal discharges. Subsequent theoretical analysis of networks of interneurons has shown that strong synchronization by mutual inhibition is only moderately robust against neuronal heterogeneities (Wang and Buzsáki, 1996) and synaptic noise (Tiesinga et al., 1998). In strong synchronization all the neurons fire with a short time-interval from each other.

In most experiments to date one measures the activity of one neuron or a small population of neurons. Periodic oscillations (extracellular or subthreshold intracellular) measured in these experiments are consistent with strong as well as weak synchronization. In weak synchronization the *average* neuronal activity is periodic, without each individual neuron having to fire at each period. Often theoretical analyses, however, have focused on strong synchronization. Here we conjecture that weak synchronization is robust against neuronal heterogeneities and synaptic noise and consequently is much more likely to occur in neuronal systems. Furthermore, we show that it can encode more information compared to strongly synchronized states. We present numerical results of weak synchronization in a simple model of a network of thalamic neurons that supports our conjecture. We use a thalamic network as an example due to the wealth of modeling information that is already available. The mechanism we discuss here, however, has more general applicability.

The thalamus acts as a relay for most of the sensory information that travels to cortical structures. It regulates sleep-wake cycles (Steriade et al., 1993), and it may be involved in early stimulus binding (Sillito et al., 1994). The lateral geniculate nucleus (LGN) and thalamic reticular nucleus (TRN) that are involved in vision have been studied extensively. Neurons of the thalamus express low-threshold calcium currents (Jahnsen and Llinás, 1984), and they rebound after a sustained hyperpolarization. It has been shown experimentally and in model calculations that inhibitory neurons can synchronize neuronal discharges in the thalamus (Wang and Rinzel, 1993; Wang et al., 1995; Golomb and Rinzel, 1994b; von Krosigk et al., 1993; Bal et al., 1995) and produce traveling waves (Rinzel et al., 1998; Destexhe and Sejnowski, 1996; Destexhe et al., 1996; Golomb et al., 1996; Tiesinga et al., 1998).

The hallmark of weak synchronization is multimodal interspike interval (ISI) histograms (ISIH). The ISI occurs only near multiples of a particular timescale, such as the period of the population activity T. Multimodality of the ISIH has been observed in the LGN (Funke et al., 1996), and it was attributed to the action of inhibitory neurons. Multimodal ISIH have also been found in model simulations of coupled inhibitory networks in the presence of noise (Golomb and Rinzel, 1994a) and in systems exhibiting stochastic resonance (SR) due to a periodic drive (Wiesenfeld and Moss, 1995). A theoretical mechanism for autonomous stochastic resonance (ASR) was proposed in a recent paper (Longtin, 1997). There the periodic drive was replaced by a periodic mode in an internal kinetic variable, such that the spikes ride on top of subthreshold voltage oscillations. In our work the periodic neuronal activity in the noise-driven system is self-induced by the network. This mechanism is absent in unconnected single neurons, or in a single element with autosynaptic feedback.

It has been suggested that the brain may encode information through an ensemble or cluster of neurons that fire within a short time of each other (Stopfer et al., 1997; Riehle et al., 1997). A particular neuron may be part of a cluster for a few cycles before it joins another neuronal ensemble. This type of dynamics is very similar to the neuronal clusters that form in our model simulations described below. An important problem is how to quantify the information content of these binding-like cluster states. The Shannon entropy has been used as a measure of information content in investigations of sensory neurons in, for instance, crickets (Levin and Miller, 1996), and flies (Rieke et al., 1997). It is, nonetheless, not known how the brain processes information, and thus it is not clear whether the Shannon entropy is the correct quantity for this purpose. It does, however, provide an upper bound on the theoretical information content of spiking neurons. It also implies that noise in the nervous system contains information and that noisy neurons are transmitting more information compared to regular noiseless spiking neurons. We emphasize that this statement is still controversial (Softky and Koch, 1993; Shadlen and Newsome, 1994; Shadlen and Newsome, 1998) because even if the entropy measure yields consistent results in sensory systems this does not guarantee its relevance to the central nervous system. With these caveats in mind we still proceed to characterize the information content of our neural networks by calculating its well-defined Shannon entropy.

One would like to calculate both the output entropy of the model system and the mutual information. The mutual information quantifies how the ensemble of outputs is related to one of the possible realizations of the input (Rieke et al., 1997), and it involves additional averagings over a conditional probability distribution,

which makes it very hard to calculate. Even the simpler calculation of the Shannon entropy from its definition in terms of the spike times is a difficult calculation. Here we shall focus on the Shannon entropy of the neuronal output of a neuron as part of the complete network. We also present here some approximations that allows us to estimate the Shannon entropy using the interspike interval time series.

2. Methods

2.1. *Network Model*

Our single-neuron model equation contains a low-threshold calcium current I_{Ca}, a general leak current I_L, a synaptic current I_{syn}, and a noise current $C_m\xi$,

$$C_m \frac{dV}{dt} = -I_{Ca} - I_L - I_{syn} - C_m\xi, \qquad (1)$$

together with the first-order (Hodgkin-Huxley type) kinetic equations for the activation m and inactivation h variables for I_{Ca} and the synaptic variable s. This yields a neuronal dynamics in terms of four variables, V, m, h, and s. We have used the kinetics for I_{Ca} and I_{syn} as specified in (Rinzel et al., 1998) (a detailed description of the model is given in Appendix A). Our single-neuron model captures some important features of the dynamics of thalamic neurons, in particular its post-inhibitory rebound (PIR). We are presently studying a more complete model, incorporating thalamocortical relay neurons and GABAergic thalamic reticular neurons (Destexhe and Sejnowski, 1997), including all the relevant active currents (Huguenard and McCormick, 1992; McCormick and Huguenard, 1992). Our preliminary results suggest that this does not change the conclusions of our discussion here.

The neurons in our network are connected all-to-all by inhibitory GABAergic synapses. Previous studies (Destexhe et al., 1996; Golomb et al., 1996; Rinzel et al., 1998) have shown that the precise spatial connectivity is important for the activity propagation. In this work, we will not consider the spatial characteristics of the neuronal activity. We have studied different sized systems, varying from $N = 1$ (a single neuron with autosynaptic feedback) to $N = 1000$. We also have included two types of noises in our model, either Gaussian current noise, characterized by $\langle\xi\rangle = 0$ and

$$\langle\xi(t)\xi(0)\rangle = 2D\delta(t), \qquad (2)$$

with D the strength of the noise, or with Poisson distributed excitatory postsynaptic potentials (EPSPs) and inhibitory postsynaptic potentials (IPSPs). In our previous work we have shown that these two types of noises are not fully equivalent (Tiesinga and José, 1999). Both can generate, however, similar statistics, and theoretically Gaussian noise is easier to control and vary. The results presented here are thus obtained with Gaussian noise. Unless stated differently the physiological total synaptic conductance used is $g_s = 2$ mS/cm^2, and the decay time of the synaptic channel $\tau_s = 16$ ms. The noise strength D is expressed in units of mV^2/ms, time in ms, currents in μA/cm^2, and voltage in mV.

The resulting differential equations for V_i, m_i, h_i, s_i are numerically integrated using a noise-adapted second-order Runge-Kutta algorithm (Greenside and Helfand, 1981) with a time-step $dt = 0.1$ ms. The calculation starts with random initial conditions, with the initial voltage chosen from a uniform distribution with a range of 20 mV centered around -68 mV, and m, h, and s are set equal to their asymptotic values for a given value of V.

2.2. *Calculated Quantities*

The raw model output are the time-traces for V_i, m_i, h_i, and s_i. The spike-times are defined as the time when the voltage V_i crosses -30 mV from below. We determined the standard histograms of interspike intervals (Rodieck et al., 1962). The instantaneous firing rate, or frequency f, is defined as the number of action potentials per second in a bin of 2 ms. Both the ISI histogram and f are averaged over all neurons in the network. We also calculated

$$v_{syn} = \frac{1}{N}\sum_i s_i, \qquad (3)$$

which is proportional to the current drive due to the synaptic connections with other neurons (and itself). Because the network is connected all-to-all, v_{syn} is the same for each neuron and represents an averaged or mean field type drive. During a periodic oscillation v_{syn} varies from its minimum value just before firing to its maximum value just after firing. The value $v_{syn} = 0.01$ is reached every cycle, except in the presence of strong noise. In that case the disperse nature of the firing creates a background value of v_{syn} above 0.01. The variable h determines the excitability of the neuron, and the state of the network strongly depends on the h-value

distribution. To determine the h-distribution prior to firing we sample h at the time that v_{syn} crosses 0.01 from above. We have determined both the instantaneous as well as the time-averaged distribution of h.

We have quantified the network's spiking activity by determining the period and periodicity of the neuronal discharge. We first determine the number n_i of neurons firing in a particular cycle i and their average spiking time t_i. The period is the average over all cycles i of $t_{i+1} - t_i$. The periodicity is then defined as N/n, where n is the average of n_i over all cycles, and N is the number of neurons in the network. For a zero noise periodic cluster state, the periodicity corresponds to the number of cycles between consecutive spikings of a particular neuron. In stochastic cluster states N/n can take non integer values.

We have also determined return maps of the interspike intervals. In the first return map we plot the next ISI_{n+1} versus the current ISI_n, whereas in the second return map we plot ISI_{n+2} versus ISI_n. We subsequently average over all neurons in the network. To obtain the corresponding transfer matrices, T and T_2, respectively, of the presumed Markov process, we divided the return map into a two-dimensional set of bins b_{ji}. The bins are centered on multiples i, j of the cycle length, and their width is also equal to the cycle length, then

$$T_{ji} = b_{ji} \Big/ \sum_i b_{ji}. \tag{4}$$

3. Results

The model considered here contains an inward low-threshold calcium current, I_T, that initiates the calcium spikes (Zhan et al., 1999). It is inactivated at the resting membrane potential (RMP, equal to −65.57 mV), and it is deinactivated at hyperpolarized voltages. For the neuron to be excitable, h has to be deinactivated (that is $h > 0.305$). We illustrate this in Fig. 1A. There are two V null-clines drawn, one (I) in the absence of a current, and the other (II) in the presence of a constant hyperpolarizing current $i = -1$ μA/cm^2. We apply a short

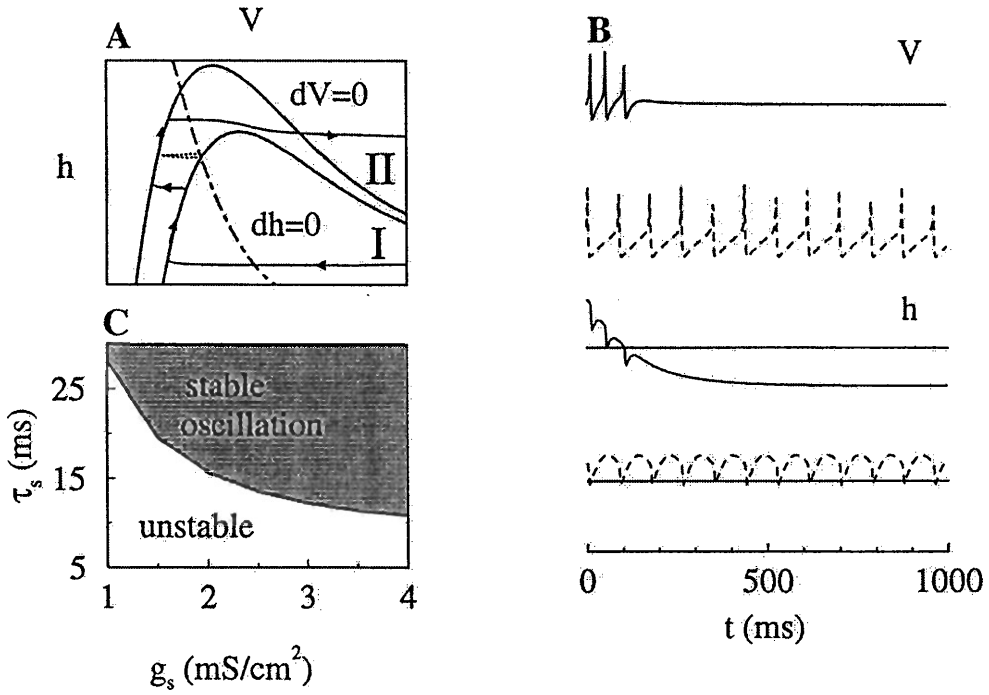

Figure 1. **A:** Phase-plane plots of the neuronal dynamics for the variables h and V. The plotted nullclines correspond to $dh/dt = 0$ (dot-dashed line), and $dV/dt = 0$ (solid lines), $I = -1.0$ (top) and $I = 0.0$ (bottom). The phase trajectory of a neuron released after 10 ms (dotted), and 200 ms (dashed) from a hyperpolarizing current pulse $I = -1$. **B:** Top curves for V, and bottom curves for h, plotted as a function of time for $\tau_s = 5$ ms $< \tau_c$ (solid lines), and curves $\tau_s = 16$ ms $> \tau_c$ (dashed lines), both with $g_s = 2.0$. The horizontal lines represent the value $h = 0.305$. **C:** Phase-diagram τ_s vs. g_s. Stable oscillations for $\tau_s > \tau_c(g_s)$ are shaded while the unstable ones $\tau_s < \tau_c(g_s)$ are colored white (see main text for details).

(10 ms) and a long pulse (200 ms) with strength i. The phase point moves to II, and the h value starts increasing with time-scale $\tau_1 = 500$ ms (see Appendix A). On termination of the short pulse the phase point moves back to I, without generating a spike. When the long pulse ends, however, the h-value is too high, and the phase point misses the nearby branch of I and generates a calcium spike.

The necessary hyperpolarization is supplied by the inhibitory postsynaptic potential (IPSP) generated by the activity of other neurons in the network. The strength of the IPSPs is determined by the value of the synaptic conductance g_s and the decay time τ_s. The critical value for periodic oscillations is defined as $\tau_s = \tau_c(g_s, N)$, which depends on the number N of neurons in the network. For $\tau_s < \tau_c$, the oscillation dies out after a finite number of action potentials. In Fig. 1B we show the voltage trace oscillations below and above threshold for $N = 1$ (single neuron with autosynaptic feedback). At the start of the simulation the neuron is released from a hyperpolarized voltage. For subthreshold values of τ_s the neuron produces a few spikes before returning to RMP. During each spike the average h value decreases, since the inhibitory drive is not strong enough to replenish the loss due to the depolarization of the spike. Above threshold a periodic spike train is produced. The h-value varies periodically, it decreases during the spike, and it increases during the inhibition. The subthreshold spike train has therefore a much smaller ISI compared to the one above threshold. We have determined the boundary between stable and unstable oscillations as function of g_s (Fig. 1A). The terms *stable* and *unstable* refer to the stability of the spiking limit cycle reached from a hyperpolarized initial condition. The minimum duration τ_s of the IPSP needed for deinactivation increases for weaker synaptic coupling g_s. The region of stability in Fig. 1C is also bounded from above. For larger values of τ_s the firing rate decreases with increasing τ_s, until the firing stops (at $\tau_s = 390$ for $g_s = 2$). These large values for τ_s are not further considered in this article. We have not systematically varied the parameters τ_0 and τ_1 (see Appendix A). However, we find that increasing τ_0 moves the $\tau_s(g_s)$ boundary downward, whereas increasing τ_1 moves it upward. The situation for a real network ($N > 1$) is more complicated, since the initial voltages play an important role. If, for instance, we would start with neurons clamped at their resting membrane potential nothing will happen. To obtain a spiking network state we therefore always start the simulations with part or all the neurons clamped at hyperpolarizing voltages. With uniform initial conditions all neurons are clamped at the same voltage value. The threshold τ_c for self-sustained oscillations is then equal to the one for a single neuron (Fig. 2A). Above threshold this network is in a coherent state: all neurons spike at the same time. For random initial conditions the initial voltage is chosen from a uniform distribution with a range of 20 mV around a hyperpolarized average value. In that case the network can sustain stable oscillations for lower values of τ_s (Fig. 2B). The network settles in a state where groups of neurons fire simultaneously. It is easy to understand why such cluster states emerge. Starting from random initial conditions each neuron will have a different phase and will thus reach the spike threshold at a different time. The first neurons to fire will cause an inhibition that blocks other neurons (further from threshold) from firing. They can fire only after the decay of the inhibition (a few τ_s). Periodic oscillations in the network are sustained by inhibition waves produced by the activity of deinactivated neurons. The oscillations automatically become coherent, with the initial phase differences between cluster neurons driven to zero. In the simplest cluster state each neuron fires with the same ISI. The time between consecutive cluster firings, or cycle length, may vary since the strength of inhibition depends on the cluster size. Neurons will fire only when v_{syn} is below a certain value: the higher the initial value (proportional to cluster size), the longer it takes to decay to this value. The precise threshold value of v_{syn} depends on state variables such as h. For higher h-values the neuron can fire at higher values of v_{syn}. More complex cluster states may also contain neurons that fire with different frequencies.

Sufficiently strong noise can induce and maintain a spiking network state even for $\tau_s < \tau_c$. Again we have to distinguish between single neurons and a network. The noise-induced dynamics of a single neuron with autosynaptic feedback will not yield a periodic spike-trace. Instead, the ISI distribution has a peak for short times due to ISIs within the spike trains and an exponential distribution for the intervals between the end of one and the start of another spike train. We show some representative voltage traces in Fig. 3C. Close to threshold and with weak noise the neuron produces a long transient that dies out eventually. Stronger noise can spontaneously induce a spike. The inhibition induced by the spike then manages to produce a short spike train. The number of spikes in this train depends

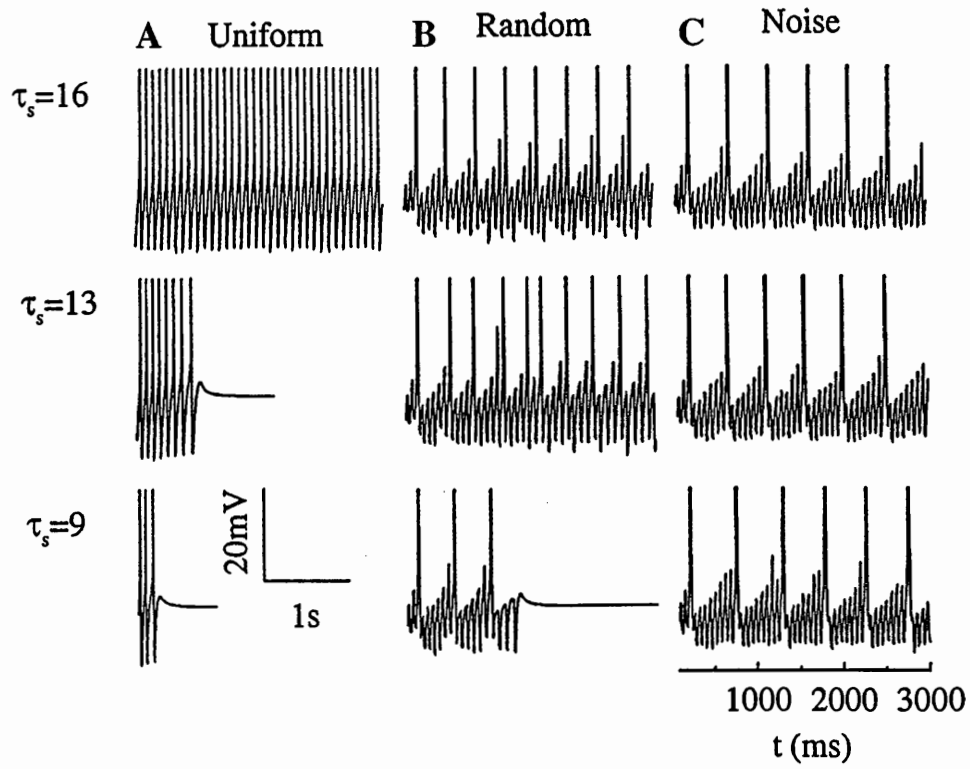

Figure 2. Voltage traces for neuron one of an $N = 1000$ neuron network of all-to-all connected with (**A**) uniform initial conditions, (**B**) random initial conditions, (**C**) uniform initial conditions with noise ($D = 0.02$, here a transient of 100 ms was discarded), for three different values of $\tau_s = 16, 13, 9$ (from top to bottom). A voltage and time scale bar is shown in the lower left graph.

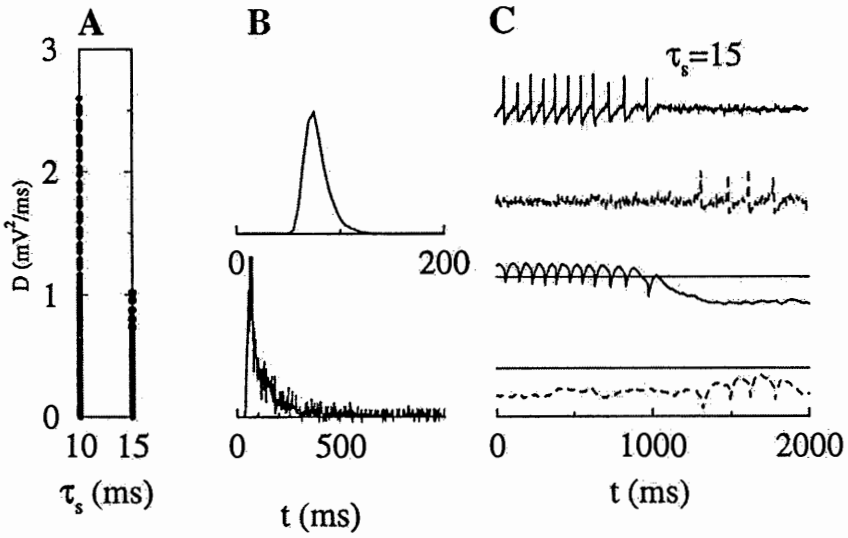

Figure 3. Noise-driven single neuron dynamics with autosynaptic feedback. **A:** Phase-diagram of neuronal behavior as a function of noise strength D, for different values of τ_s. No activity (solid line), spontaneous single spikes (dashed line), spontaneous spike-trains (filled circles). **B:** ISIH for (top) $\tau_s = 15$ and $D = 0.76$; (bottom) $\tau_s = 10$ and $D = 2$. **C:** Representative voltage (top) and h (bottom) time traces for $D = 0.26$ (solid lines) and $D = 0.76$ (dashed lines) with $\tau_s = 15$.

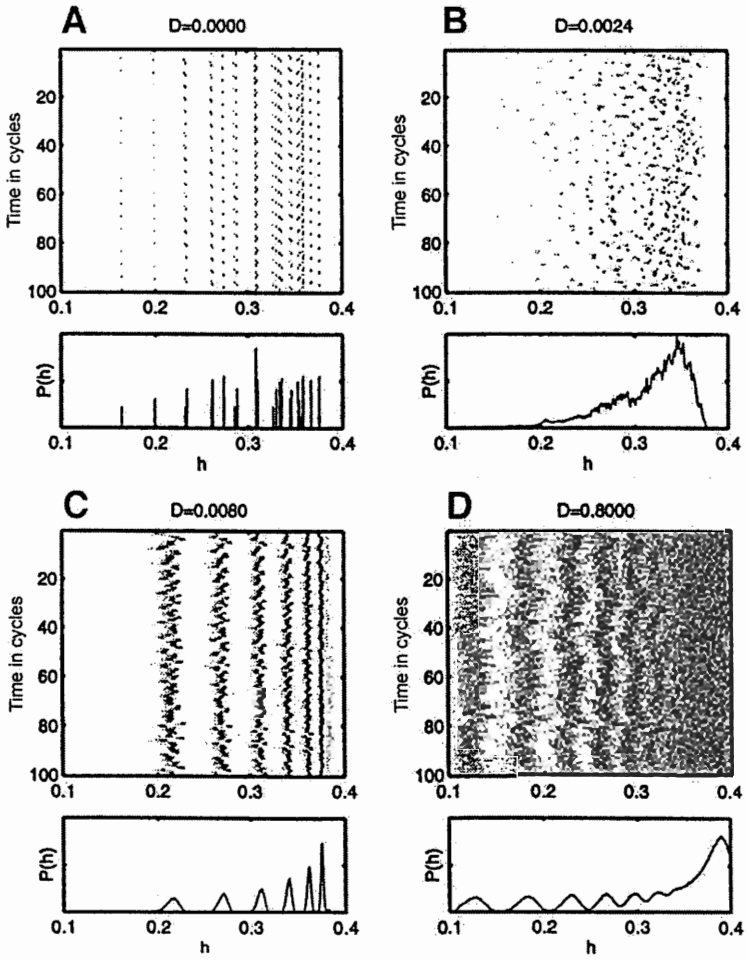

Figure 4. Each panel consists of a gray-scale coded instantaneous h value distribution for consecutive cycles (top) and the time-averaged h distribution (over at least 500 cycles) (bottom). From left to right, top to bottom, the noise-values are $D = 0$, 0.0024, 0.008, 0.8. In the upper left panel (**A**) the delta function peaks in the h-distribution have been broadened to enhance visibility.

on the distance from threshold. This makes the dynamics discussed here essentially different from stochastic resonance, since in that case one would obtain a multimodal distribution, with peaks at multiples of the driving frequency.

We studied the dynamics of the cluster states in a network with $N = 1000$, in terms of the variables shown in Figs. 4 and 5. We focused on four values for $D = 0$, 0.0024, 0.008, and 0.8. An important variable in our analysis is h, the inactivation variable of I_T, since the model neuron is excitable only when h is large enough. The distribution of h values in the network will tell us which neurons are excitable and which ones need to be deinactivated by further inhibition cycles. The regularity of the network dynamics is further reflected in the periodicity of f and v_{syn} (Fig. 5) and their autocorrelation function (not shown). Note that v_{syn} itself acts as a drive on the neurons. A higher value of v_{syn} leads to a higher threshold for spike initiation. As a consequence the larger the distance between peak and through of v_{syn}, the more noise is needed to spike out of sync.

We can identify four different types of regimes. For zero noise (D = 0) the system is in a state with five clusters of unequal size. The distribution of cluster sizes is determined by the initial conditions. At each time a neuron can only have one of five h-values. This set of h-values goes through a modulation with a period of five cycles (Fig. 4A). The derived quantities V, h, v_{syn}, and f (Fig. 5A) go through the same modulations. When all the clusters have the same size, there are no such modulations, and the h histogram would consist of only 5 peaks.

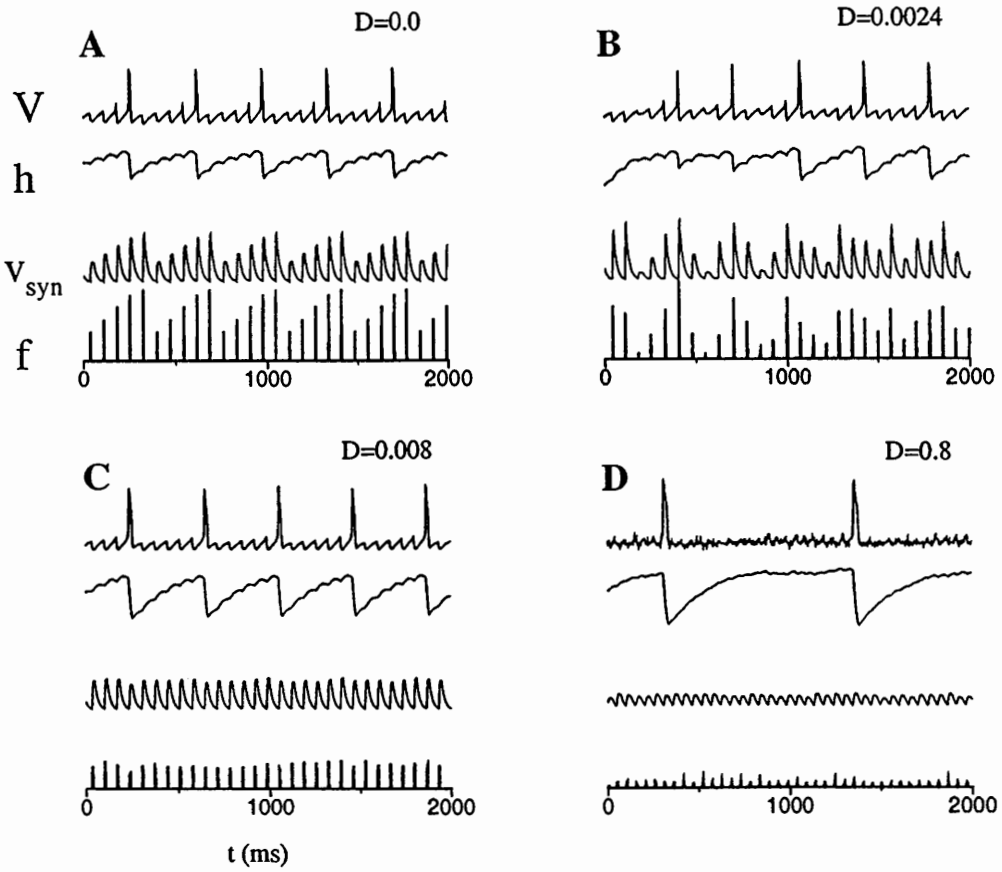

Figure 5. Four panels with the same D values given in Fig. 4: from left to right, top to bottom, the noise-values are $D = 0, 0.0024, 0.008, 0.8$. We plot in each panel from top to bottom the V and h functions of neuron one, the population average v_{syn} of the synaptic variables s_i, and the instantaneous firing rate f as a function of time.

Immediately after firing, the neuron is partially deinactivated with each subsequent cycle until it is excitable again (see the h time traces in Fig. 5). The neuron then has to wait its turn to become disinhibited and fire before other clusters do. When there is noise, there is dispersion in the spike firing times. In the absence of time delay there is only a short time interval during which neurons can fire before the inhibition blocks all other firings during one cycle. As a result, clusters lose neurons whose spike has been noise delayed, and other clusters gain those neurons as members. In addition, noise can cause neurons to fire before the rest in their cluster.

Weak noise (D = 0.0024) disorders the system. The network starts out with unequal cluster sizes (due to the initial conditions). Large clusters lose more neuron members than smaller ones. Weak noise, however, is not strong enough to equalize their numbers on the time-scale considered (5×10^4 ms). Instead the cluster sizes start to vary in a somewhat stochastic fashion, leading to an erratic firing rate (Fig. 5B) and a fluctuating period. The time-averaged h histogram is very broad (Fig. 4B).

For stronger noise (D = 0.008) the average cluster size becomes stationary after a brief transient. The h-values that the neurons of different clusters cycle through are, on the average, the same. As a result there are six smooth peaks in the h-histogram. The peaks become sharper for more deinactivated values, and the h-distribution is stationary (on the average it is the same for each cycle). The actual neurons that fire in each cluster changes with time. This state is stable up to a noise strength of approximately D = 1 (for N = 1000).

The cycle-to-cycle fluctuations in cluster sizes increases with increasing D. The inhibition that each cluster receives (proportional to v_{syn}) varies, and as a

result the width of the peaks in the h histogram increases. The cluster size also decreases with increasing D, and the amplitude of v_{syn} oscillations also decreases. The stability of a cluster can be defined as the fraction of neurons that are still part of a given cluster the next time it fires. This is related to the number and weight of the peaks in the ISIH, and it decreases with D. The neuron spends most of its time in an excited state (flat part of $h(t)$, Fig. 5D) waiting for its noise-induced spike threshold to fall in the inhibition free window. For that reason it is unlikely to fire with the same cluster as in the previous time. Finally, for larger noise strengths, $D > 1$, the firing is no longer organized in clusters (not shown), since the noise has become so large that during an inhibition free window not enough neurons fire coherently to create a large enough inhibition to block the discharge until the next cycle. As a result there are no quiescent periods defining cycles and no distinct cycles either.

The cluster states can be quantitatively described by the average cycle length (period) and the periodicity (number of cycles) of the response (see Methods). We have studied these two quantities as a function of D for different values of τ_s for N = 1000 and for different system sizes for $\tau_s = 16$ (Fig. 6). For smaller τ_s the amount of inhibition available for deinactivation is lower, and the periodicity increases since the deinactivation has to be spread out over more cycles. The cycle-period, being proportional to τ_s, also decreases. In addition, the oscillation needs a higher minimum value of D to sustain itself, since the average cluster size is given by the system size over the periodicity. When it becomes too small, the periodic component in the inhibition becomes too small, and as a result the cluster state dies. The noise strength for which this happens is only weakly dependent on τ_s. Note that the periodic component is proportional to the cluster size normalized by the network size; in addition, it decreases with increasing jitter. There is, however, a difference between large networks ($N \sim 1{,}000$) and small ones ($N \sim 10$). For small networks, a single neuron can provide enough inhibition to block neuronal discharge and thus to maintain a periodic network state. The state is very robust against noise, even when noise reduces the cluster to its minimum size (one neuron), it can still maintain a spiking state. The drawback is that the fluctuations in cluster size will be of the order of the cluster size itself, causing the cycle length to vary considerably. Below threshold (not shown) the amount of noise needed to induce a spiking state increases, and for very small networks ($N < 4$) failure can occur—that is, the network becomes quiescent if one neuron fails to fire. Note that the maximum periodicity that the system can sustain is bounded by the system size. In Fig. 6 we see that the periodicity obtained for a given D decreases with N.

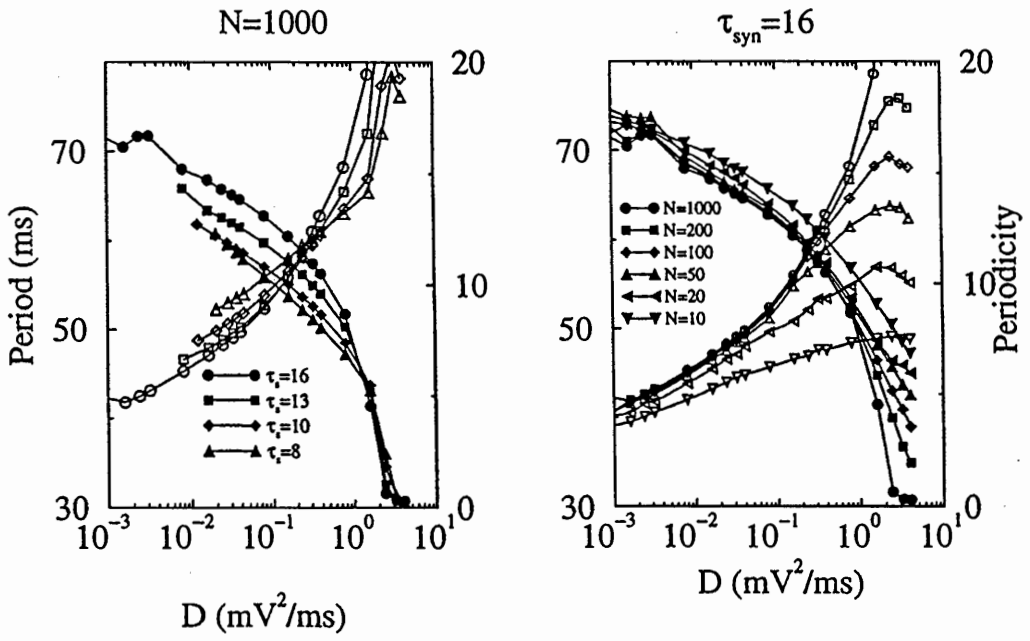

Figure 6. Here we plot the average period (filled symbols, left hand scale), and the periodicity (open symbols, right hand scale) as a function of D, for $\tau_s = 8$, 10, 13, 16 (for $N = 1000$) and for different system sizes $N = 10$, 20, 50, 100, 200, and 1000 (for $\tau_s = 16$).

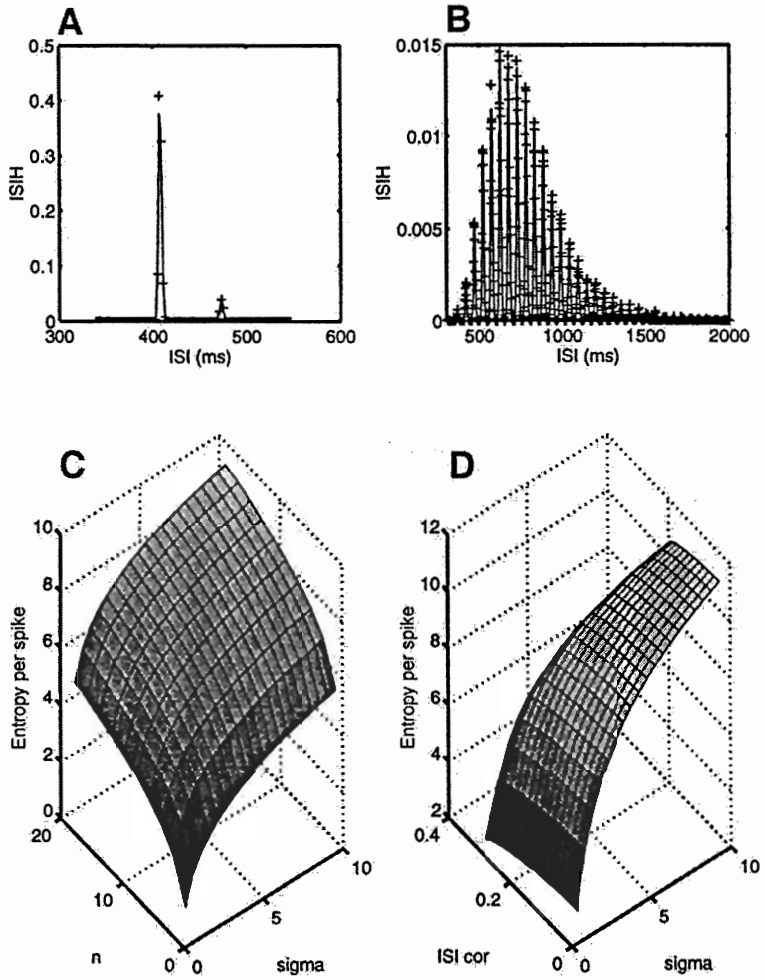

Figure 7. We plot the ISIH (+) and the corresponding SOG fitting function (continuous line) for **(A)** $D = 0.008$ and **(B)** $D = 0.8$, both for $N = 1000$, and $\tau_s = 16$. We show the entropy per spike **(C)** as a function of the number of states n and the jitter sigma and **(D)** as a function of the amount of correlation between consecutive ISI (ISIcor) and sigma.

We now discuss the possible information content of the ISI time series of individual neurons. We assume that the states are characterized by a periodic population activity. This is reflected in the ISI time series because the ISI will only take values close to multiples of the cycle length. The ISIH will therefore consist of a series of peaks. If a neuron would consistently spike with the same cluster, there would be only one peak. The peak with maximum weight is close to the average ISI (and periodicity) of the network, and the other peaks correspond to the ISI where the neuron changed cluster. The relative weight of the maximum peak is thus a measure of the stability of the clusters. In Fig. 7A and B we show the ISIH of a state with stable and unstable clusters, respectively. The width of each peak represents the jitter around a multiple of T. We find that the ISIH of an individual network neuron is to a very good approximation the same as the population averaged ISIH. This does not mean that all the neurons fire independently, it only states that all individual neurons have identical properties and that in the long run the statistics of their time-series are the same. Our analysis is therefore performed on the population averaged ISIH, and we also use the population averaged return map. We find that the ISIH is well described by a sum of Gaussians (SOG) of different widths (see Appendix B) and that the width increases with the the peak number. In Appendix B we derive an expression given in Eq. (13) for the entropy of the SOG. We see that the number of peaks and their weight –cluster

hopping– and their width –jitter within the cluster– yield two distinct contributions to the information encoding capacity. In Fig. 7C we plot the entropy as a function of width σ (taken constant for all peaks) and the total number of n peaks (weighted with a cosine envelope, Eq. (17)). In our simulations we find that the amount of jitter and the number of peaks are closely correlated and grow with D.

Our present entropy calculations assume that there is no correlation between consecutive ISIs. For a given amount of correlation γ (see Appendix B) the entropy per spike will decrease. We have quantified this in a model calculation for $n=2$ and various amounts of correlation γ (see Fig. 7D).

We have analyzed the sequence of ISIs for $D=0.008$ to ascertain whether and to what extent it can be considered to be a Markov process. We have chosen a low noise level since in that case one would expect to find the largest correlations. In Fig. 7A we show the ISIH, and in Fig. 8A the corresponding first return map. The ISI dynamics can, to a good approximation, be considered as a two-state system. As explained in Appendix B, the transfer matrix can then be parametrized by p (the weight of the largest peak) and by δ. The latter is a measure for the deviation from a renewal process, if $\delta=0$ there is no correlation between consecutive ISIs. Other parameters entering the entropy calculation are σ_1 and σ_2, the standard deviation of the peaks in the SOG. The simulation run (including the transient) is divided in 10 blocks containing approximately an equal number of ISIs per block. We have plotted p, δ and σ_1, σ_2 in Fig. 8B–D. After an initial transient the last nine blocks yield stationary values. For a true Markov process the transfer matrix T_2 for the second return map should be equal to the product $T \cdot T$. The p-values of the two matrices are nearly identical (Fig. 8C–D). The expected value δ_{2E} for the second return map is close to zero. The calculated value of δ_2 is indeed significantly closer to zero than δ.

A different way to look at the correlations is by considering the clusters themselves. We have then determined how many neurons from a given cluster fire with

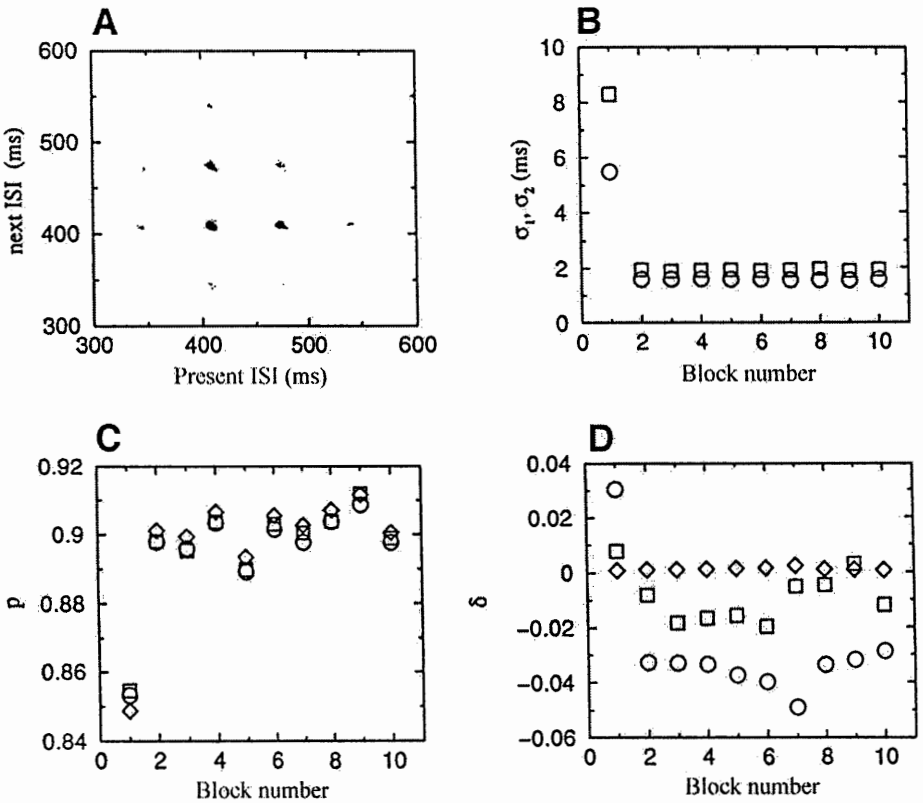

Figure 8. **A:** Return map. **B:** Variances σ_1 (circle), and σ_2 (square). **C:** Weight of first peak p. **D:** Nonrenewal parameter δ as a function of the block number. In C and D we plot the parameters for T (circles), T_2 (squares) and T^2 (diamonds). Data is for $N=1{,}000$ network, $D=0.008$. Each block contains about 14,000 ISIs.

another cluster the next time. This analysis yielded equivalent results as compared to the ISI case (not shown here).

4. Discussion

In recent years considerable attention, as well as controversy, has been directed at studying the variability of neuronal discharge in the cortex (Shadlen and Newsome, 1998). It is beyond doubt that neurons *in vivo* are noisy. The question is whether exact spike-times matter—that is, if the jitter in spike times represents information, for instance, quantified by the Shannon entropy—or if only the average firing rate matters. If spike times *do* matter, then the synchronized discharge has a special significance. An important question is whether the nervous system is sensitive to synchronization or not. Our work is relevant in shedding light to this fundamental question in two ways. We have shown that noisy neurons can synchronize without the need of a strong external drive and that the synchronized neuronal discharge has a potentially high information content. To place our results in a proper context we will now discuss these points in more detail below.

The model studied here, and other models similar to the one considered here, have been studied before by different authors. Most of these studies have been mainly concerned with a different issue—that is, the origin of spindle oscillations in the thalamus. Some of the findings in these studies are, however, of direct relevance to our article. Here we will briefly discuss the results from these studies that are of relevance to our analysis. The novel aspects of our results are discussed in the remainder of the Discussion. Golomb and Rinzel (1994a) first showed that cluster states occur in inhibitory networks consisting of neurons with a low-threshold calcium current (i_T). They also noted that noise can cause neurons to hop from one cluster to another, yielding a multimodal ISIH. This result forms the basis for the further investigation we are presenting in this article. The genesis of spindle oscillations was further studied in models that included both thalamo-cortical relays cells as well as thalamic reticular neurons with many active currents (including i_T and i_h) (Golomb and Rinzel 1994b; Destexhe et al., 1994; Wang et al., 1995). The important role of i_h in thalamic oscillations has been reviewed by Destexhe and Sejnowski (1996). Recently it was shown in experiment that a block of i_h abolishes the refractory period between active bursting states in spindles, but it does not significantly change the nature of the active state itself (Lüthi et al., 1998). This current may therefore play an important role in initiation and termination of the active states we have studied here, but it should not affect the information capacity of the active state. Kopell and LeMasson (1994) showed that cluster states also appear in models with an h-current (i_h) and standard sodium and potassium channels. They proposed that in these states the individual elements in the network and the population activity may serve different computational roles.

The role that inhibitory interneurons play in the functioning of the nervous system has long been unclear. It is hard to find, and to record from interneurons, because they are rather small. Moreover the output of the nervous system is mostly generated by the principal neurons, so early investigations studied mainly the pyramidal neurons. In recent years it has become clear that inhibition plays a major role in synchronizing principal neurons in, for example, the hippocampus (Traub et al., 1996), the thalamus (Steriade et al., 1993), and the locust olfactory system (MacLeod and Laurent, 1996). The mechanism by which synchronized oscillations are generated in the brain is only partly understood. *In vivo* many different rhythms of different frequency have been observed. Pharmacological manipulations of slices in *in vitro* experiments have elucidated some aspects of the synchronization mechanism. For instance, Traub and coworkers (Whittington, et al., 1995; Traub et al., 1996) showed that $GABA_A$-mediated inhibition is responsible for the synchronization in hippocampal slices. Slice experiments, however, suffer from the drawback that the natural afferents are cut, and therefore the synaptic activity giving rise to the *in vivo* variability is absent. Recent theoretical work has shown that in fact synchronization by mutual inhibition is not robust against neuronal heterogeneities (Wang and Buzsáki, 1996) and synaptic noise (Tiesinga et al., 1998). In theoretical investigations one usually only considers strong synchronization. In strong synchronization one imposes the strong constraint that each neuron has to fire within a short interval from each other. Here we propose that weak synchronization may in fact be more prevalent in networks connected by chemical synapses. In weak synchronization the *average* neuronal activity is periodic, without each individual neuron having to fire at each period. Weak synchronization is for example consistent with the experiments in (Traub et al., 1996). There are exceptions. For example, recent experiments on weakly electric fish show that neurons in the pacemaker nucleus are

strongly synchronized (Moortgat et al., 1998). There, however, synchronization can possibly be attributed to electric gap junctions.

Weak synchronization is associated with a periodic drive. This drive is either generated externally, as is the case with stochastic resonance (Wiesenfeld and Moss, 1995; Gluckman et al., 1996), or it is generated intrinsically by the network as it happens here. The neuron then skips periods, which it can either do deterministically (usually one peak in ISIH), or stochastically (multimodal ISIH). In both cases the network dynamics consists of clusters of neurons firing together. But in the latter case the neuronal composition of the clusters varies with time. A neuron that at a certain point fired with a certain cluster A can fire the next time with another cluster B. This mechanism yields a synchronization that is robust against noise, and neuronal heterogeneity.

Oscillating neural assemblies do play an important role in the functioning of the invertebrate nervous system. In a series of seminal experiments on the bee and locust olfactory system, Laurent and Davidowitz (1994) have shown that different odors activate overlapping ensembles of projection neurons. The periodic discharge of the ensembles is coherent on a cycle-by-cycle basis. Odors may be classified from the temporal firing pattern of projection neurons (Wehr and Laurent, 1996). Synchronization of the projection neurons may be abolished by applying picrotoxin and without changing their individual response characteristics (MacLeod and Laurent, 1996). This desynchronization was shown to impair the ability of bees to distinguish two closely related odors (Stopfer et al., 1997), and subsequently a population of neurons was found that was sensitive to the synchronization of projection neurons (MacLeod and Laurent, 1998). The ability to distinguish between two odors, based on their spike trains, was then reduced under desynchronized conditions.

We find that the information content, defined by the Shannon entropy of the spike-time distribution, contains three contributions. First, the jitter in the spike times around the cluster firing time. Second, the distribution of the number of cycles between two consecutive spikes, and finally the correlation between consecutive ISIs. Our analysis has been performed on the (average) output of a single neuron. One has to await the development of fast computational techniques to tackle the more challenging problem of quantifying the information output of the network, while taking into account the correlation in spike times between different neurons due to the cluster state. Our single-neuron spike-train results, however, may have direct relevance to recent experimental work on striatal neurons (Stern et al., 1998). Striatal neurons can be in the down (hyperpolarized, quiescent) or in the up-state (depolarized, noisy). The transitions to the up-state are precisely timed and synchronous. The fine-structure in the spike train is asynchronous. Stern and coworkers (1998) have suggested that the brain may use these two channels to encode different types of information.

The issue of information content of synchronized oscillations in thalamus has not been considered before. Very recently, however, investigators considered the information encoding of visual stimuli by bursts (calcium spikes) in the lateral geniculate nucleus of thalamus (Reinagel et al., 1999). They determined both the information capacity (our Eq. (13)), the transmitted information, and their ratio (the coding efficiency). They found that burst considered as unitary events code for about 1.4 bits of information per burst at a time scale of 4.96 ms. The coding efficiency increases with the stimulus variance. Our information capacity (Fig. 7) takes values between 1 to 10 bit per spike at a shorter time scale of 1 ms, and is consistent with their results. Additional work (Zhan et al., 1999) suggests that the calcium spikes have a similar all-or-none character as conventional sodium/potassium action potential. This lends further support to the putative role of bursts in information coding. Our work shows the effects of synchrony and correlation on information capacity. This could not be addressed experimentally (Reinagel et al., 1999).

We have studied the dependence of these oscillations on network parameters. We find that there is difference between small (around 10 neurons) and large networks (a few hundred neurons), under the conditions of having a fixed total synaptic drive per neuron. For small networks one needs more noise to drive the subthreshold network into stable oscillations. These oscillations are very robust against increases in the noise level, and the fluctuations in the time between two cluster firings (cycle length) increases with the amount of noise. For large networks strong noise causes an instability, and the stable cluster size for a given amount of noise becomes too small to inhibit out of sync neuronal discharges. For intermediate noise-strengths the neuronal dynamics self-organizes itself into a stochastically synchronized state. We also find that the farther the network is below threshold, more noise is necessary to induce a spiking state. The mechanism to create the oscillations is due to the competition between the excitatory deinactivating and the inhibitory effect of the

same synaptic drive. Each cycle will deinactivate neurons, until they are excitable again. The neuron then has to await the decay of inhibition created by more excitable neurons. For some parameter values the latter stage is absent, and the dynamics is fully deinactivation dominated. The important time-scales in the dynamics are the deinactivation time-scale τ_1 and the synaptic decay time τ_s. The cycle or population period scales directly with τ_s. Our results therefore predict that by pharmacologically decreasing τ_s one can increase the cycle frequency.

In summary, the brain has circuitry capable of synchronizing with heterogeneous components and in the presence of noise. The spike trains of the synchronized discharge still contain information. Whether the brain utilizes this mechanism to synchronize and, more important, whether it uses the information in the precise temporal sequence are still open questions awaiting further study.

Appendix A: Model Equations

In this appendix we define the models studied in this article. The dynamics of the voltage V and the kinetic variables h, s, and m are given by the following equations:

$$\begin{aligned} C_m \frac{dV}{dt} &= -I_{Ca} - I_L - I_{syn} - C_m \xi, \\ \frac{dh}{dt} &= (h_\infty - h)/\tau_h, \\ \frac{ds}{dt} &= k_f F(V_{pre})(1-s) - s/\tau_{syn}, \\ m &= m_\infty(V). \end{aligned}$$

Here the currents are

$$\begin{aligned} I_L &= g_l(V - E_L), \\ I_{Ca} &= g_{Ca} m_\infty(V) h (V - E_{Ca}), \\ I_{syn} &= g_{syn} s_{tot} (V - E_{syn}). \end{aligned}$$

The asymptotic values of the kinetic variables, and the h time-scale, are specified by

$$\begin{aligned} m_\infty &= 1/[1 + \exp -(V+40)/7.4], \\ h_\infty &= 1/[1 + \exp(V+70)/4)], \\ \tau_h &= \phi(\tau_0 + \tau_1/[1 + \exp(V+50)/3]). \end{aligned} \tag{5}$$

The synaptic activity is implemented in a standard way (Wang and Rinzel, 1993). F is chosen such that a presynaptic depolarization higher than -35 mV will open the synaptic channels:

$$F(V) = 1/[1 + \exp -(V+35)/2]. \tag{6}$$

The total synaptic coupling in our all-to-all network is defined as

$$s_{tot} = \frac{1}{N} \sum_i s_i, \tag{7}$$

and is the same for each neuron.

The standard physiological set of parameters we use in our calculations have the conductances $g_L = 0.4$, $g_{Ca} = 1.5$, and $g_{syn} = 2.0$ (in mS/cm^2), the reversal potentials $E_L = -70$, $E_{Ca} = 90$, $E_{syn} = -85$ (in mV), and $C_m = 1$ μF/cm^2, $\tau_0 = 30$, $\tau_1 = 500$ (in ms), $k_f = 0.5$ ms^{-1}, and $\phi = 1.3$.

Appendix B: Shannon Entropy Calculation

As mentioned in the main body of the article, we quantify the information content in the ISI using the Shannon entropy,

$$S = -\int \mathcal{D}(\{t_i^n\}) \mathcal{P}(\{t_i^n\}) \log_2 \mathcal{P}(\{t_i^n\}), \tag{8}$$

for the distribution of the spiking times. In this expression t_i^n is the ith spike time of the nth neuron, and $\mathcal{D}$ is the sum over all spiking time possibilities within a $[0, T]$ interval. We do not try to evaluate this quantity for the whole network, since at present it is a very hard calculation to do. Here we will instead calculate the one neuron entropy in the network, which is expressed in terms of the distribution $P(\{\tau_n\})$ of interspike intervals τ_n, as

$$\begin{aligned} S &= -\int \mathcal{D}(\{\tau_n\}) p(\{\tau_n\}) \log_2 p(\{\tau_n\}) \\ &\approx -\langle N \rangle \int d\tau P_{ISIH}(\tau) \log_2 P_{ISIH}(\tau), \end{aligned} \tag{9}$$

with $\langle N \rangle$ the average number of events during time interval T. We also assume that consecutive ISIs are randomly independent,

$$p(\tau_1, \cdots, \tau_N) = \Pi_n P_{ISIH}(\tau_n). \tag{10}$$

As explained in the main body of the text the ISIH obtained from our simulations is, to a good

approximation, a sum of Gaussians (SOG)—that is,

$$P_{ISIH}(\tau) = \sum_i c_i G(\tau \mid \mu_i, \sigma_i), \qquad (11)$$

where

$$G(\tau \mid \mu_i, \sigma_i) = \frac{1}{\sqrt{2\pi\sigma_i^2}} \exp\left[-(\tau-\mu_i)^2/2\sigma_i^2\right], \qquad (12)$$

with average μ_i, standard deviation σ_i, and c_i is the relative weight for the ith Gaussian contribution. From the calculated ISIH, we estimate these parameters from the weight c_i, the average μ_i, and the standard deviation σ_i of the ith peak. When $(\mu_{i+1} - \mu_i) \gg \sigma_i$ for all i, Eq. (9) reduces to

$$S = \langle N \rangle \left(\sum_i c_i \log_2 2\pi e(\sigma_i/\sigma_s)^2 - \sum_i c_i \log_2 c_i \right)$$
$$\equiv S_1 + S_2. \qquad (13)$$

These are the two contributions to the entropy of a multimodal ISIH. A contribution S_1 due to the jitter around the average ISI value of a given state i (Shannon and Weaver, 1949), and the contribution S_2 due to the discrete probability distribution of the number of cycles between two spikes. Note that S_1 depends on the accuracy or scale with which the ISI can be recorded and detected (Shannon and Weaver, 1949; Rieke et al., 1997). The ISIs obtained from our simulations take values that are multiples of $dt = 0.01$. However, we have used a scale of $\sigma_s = 1$ ms, which is more comparable to the spiking precision that is obtained in experiment (Mainen and Sejnowski, 1995; Reinagel et al., 1999). In the other limit $(\mu_{i+1} - \mu_i) < \sigma_i$, we numerically evaluate the entropy from Eq. (9) using the measured (binned) ISIH.

In Eq. (9) we have assumed that consecutive ISIs are independent. If consecutive ISIs are correlated, however, one can use the theory of Markov chains to evaluate the Shannon entropy of the spike trains. The ISIs can belong to n different states, and they have an equilibrium probability $P_{eq} = (c_1, \cdots, c_n)$ to be in any particular state. From a given state i the ISI can jump to a new state j with probability T_{ji}, which we can obtain from a return map (see Methods).

When the ISIs are independent, $T_{ji} = c_j$ (that is, the next state does not depend on the previous state). The actual ISI in each state also displays some jitter, and it is distributed according to some $\phi_i(\tau)$. We will assume that ϕ_i is Gaussian (as before), and the entropy is then given by

$$S = -\frac{1}{\log 2}\Big[(m+1)I \cdot (T\alpha) \cdot P_{eq} + \sum_i c_i \log c_i + mI \cdot (T \log T) \cdot P_{eq}\Big]$$
$$\equiv S_1 + S_2 + S_3. \qquad (14)$$

We have used the following definitions: $m + 1$ is the number of ISIs, $(T\alpha)_{ij} = T_{ij}\alpha_i (T \log T)_{ij} = T_{ij} \log T_{ij}$ (no summations implied), $\alpha_i = \int d\tau \phi_i(\tau) \log \phi_i(\tau)$, and $\cdot$ denotes matrix multiplication. Here we give the explicit formula's for $n = 2$

$$(T\alpha) \equiv \begin{pmatrix} \alpha_1 p & \alpha_2(1-q) \\ \alpha_1(1-p) & \alpha_2 q \end{pmatrix}, \qquad (15)$$

$$(T \log T) \equiv \begin{pmatrix} p \log p & (1-q)\log(1-q) \\ (1-p)\log(1-p) & q \log q \end{pmatrix}. \qquad (16)$$

When the ISIs are independent then $S_3 = 0$, and S_1 and S_2 reduce to their expression given in Eq. (13).

We have evaluated expression Eq. (13) (see Fig. 7C) using

$$c_{L+1\pm i} = \frac{1}{2\pi}\left(\frac{2}{n} + \sin\frac{2\pi\left(\pm i + \frac{1}{2}\right)}{n} - \sin\frac{2\pi\left(\pm i - \frac{1}{2}\right)}{n}\right), \qquad (17)$$
$$\mu_j = \mu + (j - L)\Delta\mu,$$
$$\sigma_j = \sigma.$$

Here $n = 2L + 1, i = 1, \cdots, L; j = 1, \cdots, n$; and $\Delta\mu$ is the cycle length (period).

Correlation in consecutive ISIs can be parameterized using a δ, with $q = 1 + \delta - p$ in Eqs. (15) and (16). The resulting correlation between consecutive interspike intervals τ is defined as

$$\gamma(\delta) = \sqrt{\frac{\langle \tau_i \tau_{i+1} \rangle - \langle \tau \rangle^2}{\langle \tau^2 \rangle - \langle \tau \rangle^2}}. \qquad (18)$$

The explicit result for $m = 100$ is plotted as function of γ in Fig. 7D.

Acknowledgments

This work was partially funded by the Northeastern University CIRCS fund and the Sloan Center for Theoretical Neurobiology (PT). We thank T.J. Sejnowski and the anonymous referees for useful suggestions.

References

Bal T, von Krosigk M, McCormick DA (1995) Synaptic mechanisms underlying synchronized oscillations in the ferret lateral geniculate nucleus in vitro. *J. Physiol.* 483:641–663.

Destexhe A, Bal T, McCormick DA, Sejnowski TJ (1996) Ionic mechanisms underlying synchronized oscillations and propagating waves in a model of ferret thalamic slices. *J. Neurophys.* 76:2049–2070.

Destexhe A, Contreras D, Sejnowski TJ, Steriade M (1994) A model of spindle rhythmicity in the isolated thalamic reticular nucleus. *J. Neurophys.* 72:803–818.

Destexhe A, Sejnowski TJ (1997) Synchronized oscillations in thalamic networks: Insights from modeling studies. In Steriade M, Jones EG, McCormick DA, eds. *Thalamus*. Elsevier. Amsterdam.

Funke K, Nelle E, Li B, Wörgötter F (1996) Corticofugal feedback improves the timing of retino-geniculate signal transmission. *Neuroreport* 7:2130–2134.

Gluckman BJ, Netoff TI, Neel EJ, Ditto WL, Spano ML, Schiff SJ (1996) Stochastic resonance in a neuronal network from a mammalian brain. *Phys. Rev. Lett.* 77:4098–4101.

Golomb D, Rinzel J (1994a) Clustering in globally coupled inhibitory neurons. *Physica D* 72:259–282.

Golomb D, Rinzel J (1994b) Synchronization properties of spindle oscillations in a thalamic reticular nucleus model. *J. Neurophys.* 72:1109–1126.

Golomb D, Wang XJ, Rinzel J (1996) Propagation of spindle waves in a thalamic slice model. *J. Neurophysiol.* 75:750–769.

Greenside HS, Helfand E (1981) Numerical integration of stochastic differential equations. *Bell Syst. Tech. J.* 60:1927.

Huguenard JR, McCormick DA (1992) Simulation of the currents involved in rhythmic oscillations in thalamic relay neurons. *J. Neurophys.* 68:1373–1383.

Jahnsen H, Llinás R (1984) Ionic basis for the electroresponsiveness and oscillatory properties of the guinea-pig thalamic neurones in vitro. *J. Physiol.* 349:227–247.

Kopell N, LeMasson G (1994) Rhythmogenesis, amplitude modulation, and multiplexing in a cortical architecture. *Proc. Natl. Acad. Sci.* 91:10586–10590.

Laurent G, Davidowitz H (1994) Encoding of olfactory information with oscillating neural assemblies. *Science* 265:1872–1875.

Levin JE, Miller JP (1996) Broeadband neural encoding in the cricket cercal sensory system enhanced by stochastic resonance. *Nature* 380:165–168.

Longtin A (1997) Autonomous stochastic resonance in bursting neurons. *Phys. Rev. E* 55:868–876.

Lüthi A, Bal T, McCormick DA (1998) Periodicity of thalamic spindle waves is abolished by ZD7288, a blocker of Ih. *J. Neurophysiol.* 79:3284–3289.

MacLeod K, Laurent G (1996) Distinct mechanisms for synchronization and temporal patterning of odor-encoding neural assemblies. *Science* 274:976–979.

MacLeod K, Laurent G (1998) Who reads temporal information contained across synchronized and oscillatory spike trains. *Nature* 395:693–698.

Mainen ZF, Sejnowski TJ (1995) Reliability of spike timing in neocortical neurons. *Science* 268:1503–1506.

McCormick DA, Huguenard JR (1992) A model of the electrophysiological properties of thalamocortical relay neurons. *J. Neurophys.* 68:1384–1400.

Moortgat KT, Keller CH, Bullock TH, Sejnowski TJ (1998) Submicrosecond pacemaker precision is behaviorally modulated: The gymnotiform electromotor pathway. *Proc. Natl. Acad. Sci.* 95:4684–4689.

Reinagel P, Godwin D, Sherman SM, Koch C (1999) Encoding of visual information by LGN bursts. *J. Neurophysiol.* 81:2558–2569.

Riehle A, Grun S, Diesmann M, Aertsen A (1997) Spike synchronization and rate modulation differentially involved in motor cortical function. *Science* 278:1950–1953.

Rieke F, Warland D, de Ruyter van Steveninck RR, Bialek W (1997) *Spikes: Exploring the Neural Code*. MIT Press, Cambridge.

Rinzel J, Terman D, Wang XJ, Ermentrout B (1998) Propagating activity patterns in large-scale inhibitory neuronal networks. *Science* 279:1351–1355.

Rodieck RW, Kiang NY-S, Gerstein GL (1962) Some quantitative methods for the study of spontaneous activity of single neurons. *Biophys. J.* 2:351–368.

Shadlen MN, Newsome WT (1994) Noise, neural codes, and cortical organization. *Curr. Opin. Neurobiol.* 4:569–579.

Shadlen MN, Newsome WT (1998) The variable discharge of cortical neurons: Implications for connectivity, computation, and information coding. *J. Neurosci.* 18:3870–3896.

Shannon CE, Weaver W (1949) *The Mathematical Theory of Communication.* University of Illinois Press, Urbana and Chicago.

Sillito AM, Jones HE, Gerstein GL, West DC (1994) Feature-linked synchronization of thalamic relay cell firing by feedback from the visual cortex. *Nature* 369:479–482.

Singer W, Gray CM (1995) Visual feature integration and the temporal correlation hypothesis. *Annu. Rev. Neurosci.* 18:555–586.

Softky WR, Koch C (1993) The highly irregular firing of cortical cells is inconsistent with temporal integration of random EPSPs. *J. Neurosci.* 13:334–350.

Steriade M, Cormick DA, Sejnowski TJ (1993) Thalamocortical oscillations in the sleeping and aroused brain. *Science* 262:679–685.

Stern EA, Jeager D, Wilson CJ (1998) Membrane potential of simultaneously recorded striatal spiny neurons in vivo. *Nature* 394:475–478.

Stopfer M, Bhagavan S, Smith BH, Laurent G (1997) Impaired odor discrimination on desynchronization of odor-encoding neural assemblies. *Nature* 390:70–74.

Tiesinga PHE, José JV (1999) Spiking statistics in noisy hippocampal interneurons. *Neurocomputing* 26/27:299–303.

Tiesinga PHE, Rappel W-J, José JV (1998) Synchronization in networks of noisy interneurons. In Bower J, ed. *Computational Neuroscience*. Plenum Press, New York. pp. 555–559.

Tiesinga PHE, José JV (2000) Robust gamma oscillations in networks of inhibitory hippocampus interneurons. *Network* 11(1):1–23.

Traub RD, Whittington MA, Colling SB, Buzsaki G, Jeffreys JGR (1996) Analysis of gamma rhythms in the rat hippocampus in vitro and in vivo. *J. Physiol.* 493:471–484.

von Krosigk M, Bal T, McCormick DA (1993) Cellular mechanisms of a synchronized oscillation in the thalamus. *Science* 261:361–364.

Wang X-J, Golomb D, Rinzel J (1995) Emergent spindle oscillations and intermittent burst firing in a thalamic model: Specific neuronal mechanisms. *Proc. Natl. Acad. Sci. USA* 92:5577–5581.

Wang X-J, Rinzel J (1993) Spindle rhythmicity in the reticularis thalami nucleus: synchronization among mutually inhibitory neurons. *Neurosci.* 53:899–904.

Wang X-J, Buzsáki G (1996) Gamma oscillation by synaptic inhibition in a hippocampal interneuronal network model. *J. Neurosci.* 16:6402–6413.

Wehr M, Laurent G (1996) Odor-encoding by temporal sequences of firing in neural assemblies. *Nature* 384:162–165.

Whittington MA, Traub RD, Jeffreys JGR (1995) Synchronized oscillations in interneuron networks driven by metabotropic glutamate receptor activation. *Nature* 373:612–615.

Wiesenfeld K, Moss F (1995) Stochastic resonance and the benefits of noise: From ice ages to crayfish and SQUIDs. *Nature* 373:33–36.

Zhan XJ, Cox CL, Rinzel J, Sherman SM (1999) Current clamp and modeling studies of low-threshold calcium spikes in cells of the cat's lateral geniculate nucleus. *J. Neurophysiol.* 81:2360–2373.